

## **Characterization of dissimilar friction stir welded lap joints of AA5083 and GL D36 steel**

Batistao, Bruna Fernanda; Bergmann, Luciano; Gargarella, Piter; de Alcantara, Nelson Guedes; dos Santos, Jorge Fernandez; Klusemann, Benjamin

*Published in:*

Journal of Materials Research and Technology

*DOI:*

[10.1016/j.jmrt.2020.10.078](https://doi.org/10.1016/j.jmrt.2020.10.078)

*Publication date:*

2020

*Document Version*

Publisher's PDF, also known as Version of record

[Link to publication](#)

*Citation for pulished version (APA):*

Batistao, B. F., Bergmann, L., Gargarella, P., de Alcantara, N. G., dos Santos, J. F., & Klusemann, B. (2020). Characterization of dissimilar friction stir welded lap joints of AA5083 and GL D36 steel. *Journal of Materials Research and Technology*, 9(6), 15132-15142. <https://doi.org/10.1016/j.jmrt.2020.10.078>

### **General rights**

Copyright and moral rights for the publications made accessible in the public portal are retained by the authors and/or other copyright owners and it is a condition of accessing publications that users recognise and abide by the legal requirements associated with these rights.

- Users may download and print one copy of any publication from the public portal for the purpose of private study or research.
- You may not further distribute the material or use it for any profit-making activity or commercial gain
- You may freely distribute the URL identifying the publication in the public portal ?

### **Take down policy**

If you believe that this document breaches copyright please contact us providing details, and we will remove access to the work immediately and investigate your claim.



Available online at [www.sciencedirect.com](http://www.sciencedirect.com)  
**jmr&t**  
 Journal of Materials Research and Technology  
 journal homepage: [www.elsevier.com/locate/jmrt](http://www.elsevier.com/locate/jmrt)



## Original Article

# Characterization of dissimilar friction stir welded lap joints of AA5083 and GL D36 steel



Bruna Fernanda Batistão <sup>a</sup>, Luciano Andrei Bergmann <sup>b</sup>,  
 Piter Gargarella <sup>a,c,\*</sup>, Nelson Guedes de Alcântara <sup>a,c</sup>, Jorge F. dos Santos <sup>b</sup>,  
 Benjamin Klusemann <sup>b,d</sup>

<sup>a</sup> Federal University of Sao Carlos, Graduate Program in Materials Science and Engineering, Rodovia Washington Luiz, km 235 SP-310, São Carlos, São Paulo, 13565-905, Brazil

<sup>b</sup> Helmholtz-Zentrum Geesthacht (HZG), Institute of Materials Research, Materials Mechanics, Solid-State Joining Processes, Max-Planck-Straße 1, Geesthacht, 21502, Germany

<sup>c</sup> Federal University of Sao Carlos, Department of Materials Engineering, Rodovia Washington Luiz, km 235 SP-310, São Carlos, São Paulo, 13565-905, Brazil

<sup>d</sup> Leuphana University of Lüneburg, Institute of Product and Process Innovation, Universitätsallee 1, Lüneburg, 21335, Germany

## ARTICLE INFO

### Article history:

Received 20 August 2020

Accepted 26 October 2020

Available online 2 November 2020

### Keywords:

Aluminum alloys

Steel

Friction stir welding

Steel hook

Intermetallic compounds

## ABSTRACT

Dissimilar AA5083 to GL D36 steel welds produced by Friction Stir Welding in lap joint configuration, with the aluminum plate placed on the advancing side, are studied regarding their mechanical, microstructural and interfacial properties for varying process parameters, i.e. welding and tool rotational speed. An increase of welding speed or decrease of the rotational speed causes the formation of tunnel defects, a decrease of the steel hook height and reduction of grain size in the aluminum stir zone. The maximum hardness is observed at the weld interface, due to the presence of intermetallic compound layers, identified as the Fe-rich phases as FeAl and Fe<sub>3</sub>Al. As the rotational speed increases, an increase of the IMCs thickness in the weld interface is found, which contributes to the degradation of the lap shear strength, due to the brittleness and high hardness of these phases. Overall, the maximum lap shear strength is obtained for welds showing macro (steel hook) and micro interlocks, as well as the formation of thin IMC layers at the weld interface.

© 2020 The Authors. Published by Elsevier B.V. This is an open access article under the CC BY-NC-ND license (<http://creativecommons.org/licenses/by-nc-nd/4.0/>).

## 1. Introduction

The crescent use of hybrid structures, combining beneficial properties of the component materials, has been reported in

various industries, such as aeronautics, automotive, and marine applications. These multi-material structures can meet both the search for high-performance and weight reduction [1]. The replacement of steel parts by lightweight materials in the automotive and shipbuilding sectors has

\* Corresponding author.

E-mail address: [piter@ufscar.br](mailto:piter@ufscar.br) (P. Gargarella).

<https://doi.org/10.1016/j.jmrt.2020.10.078>

2238-7854/© 2020 The Authors. Published by Elsevier B.V. This is an open access article under the CC BY-NC-ND license (<http://creativecommons.org/licenses/by-nc-nd/4.0/>).

made hybrid structures of steel and aluminum alloys common. The excellent specific properties of the aluminum alloys attend the weight savings and fuel or energy economy and lead to the development and improvement of techniques for joining dissimilar materials [2–4].

Various methods are being proposed in the literature to join aluminum and steel [3]. For example, riveting, resistance welding, metal inert gas, and Friction Stir Welding (FSW) have successfully been used to join aluminum parts to steel components in automotive vehicles [3–6]. Besides that, in the ship-building industry, aluminum alloys are being welded to steel using transition joints, consisting of a base of steel, an intermediate layer of pure aluminum, and a corrosion-resistant aluminum layer, joined by the explosion welding process [3,4].

Among these methods, FSW is a solid-state joining process that consists of the heating and softening of the base materials by friction between the rotating tool and workpieces, and in their mixing and transportation due to the combination of rotational and translational movement of the tool [7,8]. Various studies have recently shown that this method can successfully be used in the joining of various similar and dissimilar material combinations [9–21]. Compared to fusion welding technologies, the lower temperatures in short cycle times of this process avoid solidification issues and reduce the thickness of the Intermetallic Compound (IMC) layers formed at the weld interface of dissimilar joints [22–25].

IMC layers in Al/steel joints are formed across the weld interface by the interdiffusion of the Al and Fe atoms [26] and usually result in the reduction of the ductility and tensile strength of the joint [23,26].  $\text{Fe}_3\text{Al}$ ,  $\text{FeAl}$ ,  $\text{FeAl}_2$ ,  $\text{Fe}_2\text{Al}_5$ , and  $\text{FeAl}_3$  are the most common nonstoichiometric IMCs formed during the welding of aluminum and steel [23]. Compounds such as  $\text{FeAl}_2$ ,  $\text{Fe}_2\text{Al}_5$ , and  $\text{FeAl}_3$ , with high aluminum content, are problematic due to their brittleness, while compounds such as  $\text{Fe}_3\text{Al}$  and  $\text{FeAl}$ , with high iron content, might be beneficial due to their specific strength and good wear, oxidation, and corrosion resistance properties [27].

The IMC type and size of the compounds formed at the weld interface are influenced by the welding parameters [23]. Kimapong et al. [28] identified the  $\text{FeAl}$  and  $\text{FeAl}_3$  phases at the interface of AA5083 to SS400 steel and concluded that the IMC layer thickness is increasing under higher rotational and lower welding speed, and for higher probe depth. An increase in IMC layer thickness causes the degradation of the shear strength. IMC layers thinner than 1–2  $\mu\text{m}$  are recommended for high interface strength [23].

Already some studies about dissimilar aluminum to steel FSW joints have been performed [28–32], considering the effects of different materials and process conditions on the microstructural and mechanical properties of the welds. For example, the characterization of the microstructure resultant for fixed process condition was evaluated [29], while the influence of the welding parameters on the IMC formation was the focus on another investigation [30]. The study conducted by Coelho et al. [29], focusing on the characterization of the microstructure, texture, and IMC formation, stated that the size and amount of steel particles dispersed on the aluminum stir zone (Al-SZ) determine the mechanical properties of AA6181-T4 to HC340LA steel joints, with the IMC layers acting as mechanical interlocking. Furthermore, the study

conducted by Pourali et al. [30] on the influence of the welding and rotational speed on the IMC formation, pointed out that defects, such as voids, are the cause for the deterioration of the mechanical properties of AA1100 to St37 steel joints. Xiong et al. [31] showed that thin IMCs phases and micro interlocks formed at the weld interface of dissimilar AA1100 to 1Cr18Ni9Ti stainless steel joints are responsible for the obtained high strength of these joints. Similarly, Movahedi et al. [32] illustrated that the macro- and micro-mechanical interlocking, and the metallurgical bonding at the weld interface influence the strength of AA5083 to St-12 joints. On the other hand, Kimapong et al. [28], pointed out that the formation and growth of  $\text{FeAl}_3$  layers cause deterioration of the mechanical properties in the joints.

The present research aims to investigate the influence of welding and tool rotational speed on the microstructural and interface properties of dissimilar AA5083-O/H111 to naval GL D36 steel welds produced by FSW in a lap joint configuration with the aluminum plate placed on the advancing side (AS), which is different from the configuration reported in other studies of Al/St FSW lap joints, where the aluminum plate is placed on the retreating side (RS) [3,28–30,33], or the position is not identified [31,32,34], which might be related to the positioning of the plates of Al/St FSW butt joints, where the aluminum should be placed on the RS to produce welds [35]. The influence of the micro- and macrostructural features and IMC layers on mechanical properties is analyzed. For this purpose, several microstructural and mechanical tests are employed to characterize the resulting welds in detail. To understand the effects of the process parameters on the joint properties, the microstructural and interface properties are correlated with the mechanical properties of the joints and welding parameters.

## 2. Materials and methods

The base materials (BM) used were a 4 mm thick AA5083-O/H111 and a 6 mm thick GL D36 steel plate, with the chemical composition as presented in Table 1. Spark Spectrometric analysis was used to measure the chemical composition of GL D36 steel, and ASTM B209M-14 standard is used for AA5083.

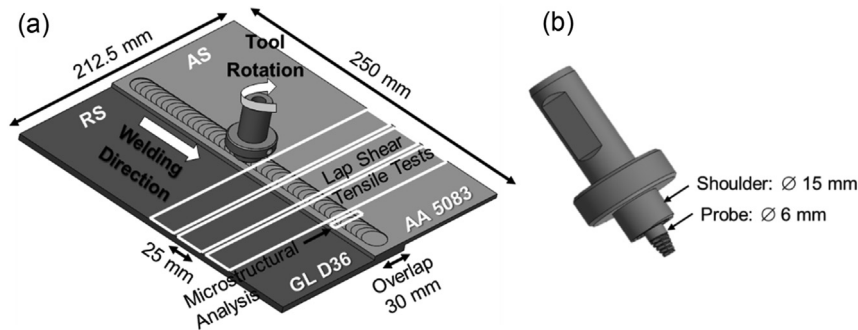
The welds were produced using a high stiffness FSW Gantry System. The used tool features a flat scrolled shoulder with 15 mm diameter and a threaded conical probe with three flats, 6 mm in diameter, and 4.2 mm in length, see Fig. 1, both made of Hotvar hot-work tool steel (2.6% Cr, 2.25% Mn and 0.85% V). The welding process was carried out in lap joint configuration, with the aluminum plate placed above the steel on the AS, 30 mm overlap, and 250 mm of weld length, Fig. 1.

The FSW process was performed using a tilt angle and an axial force fixed at 0.5° and 15 kN, respectively. The remaining process parameters, i.e. welding and rotational speed, are varied and summarized in Table 2 for the different welds.

The welds were cut transverse to the weld direction and the cross-sections were prepared according to standard metallographic procedures, i.e. ASTM E3-11. The aluminum part of the welds cross-section was electrolytically etched using a Barker reagent, and the steel part was chemically etched using a 0.5% Nital solution, followed by observations of

**Table 1 – Chemical composition of AA5083 (ASTM B209M-14) and GL D36 steel (measured by spark spectrometric analysis).**

Material	Chemical Composition (wt.%)								
AA5083	Si	Fe	Cu	Mn	Mg	Cr	Zn	Ti	Al
	<0.40	<0.40	<0.10	0.40–1.0	4.0–4.9	0.05–0.25	<0.25	<0.15	Bal.
GL D36 Steel	C	Si	Mn	P	S	Ni	Al	Cu	Fe
	0.17	0.39	1.4	0.013	<0.01	0.02	0.027	0.03	Bal.

**Fig. 1 – Schematic illustration of (a) the AA5083/GL D36 steel lap joint configuration and (b) the threaded conical FSW tool. The position for sample extraction are indicated as well.****Table 2 – Welding parameters used for joining AA5083 to GL D36 steel by FSW. The tilt angle and axial force were fixed at 0.5° and 15 kN, respectively.**

Weld Number	Welding Speed (mm/s)	Rotational Speed (rpm)
Weld 1	5	300
Weld 2	5	500
Weld 3	5	700
Weld 4	9	700
Weld 5	13	700
Weld 6	5	900
Weld 7	9	900
Weld 8	13	900

the samples in an optical microscope (OM) equipped with polarized light. The ASTM E112-13 standard was used to determine the grain size throughout the intercept method. Vickers hardness tests were carried out following ASTM E384-17 standard. Three lines of microhardness tests were conducted in each cross-section, with 0.25 mm distance between each measurement point, holding time of 10 s, and a load of 0.2 kg. Two lines were executed horizontally, one line in the aluminum part and another in the steel part, both with 1 mm distance from the weld interface, and one further line was executed vertically, in the middle of the SZ. Next to the hardness measurements, lap shear tensile tests are used to evaluate the mechanical properties. The tests were conducted perpendicular to the welding direction, using a constant crosshead speed of 1 mm/min and a separation gap between the clamps of 112.5 mm in a screw-driven testing machine with a load capacity of 100 kN at room temperature. Three samples for each weld with 212.5 mm long and 25 mm wide were employed in the lap shear tensile tests.

For the interface characterization, a Scanning Electron Microscopy (SEM) equipped with Energy Dispersive X-ray

Spectroscopy (EDS) is used to measure the size of the IMC layers, and X-ray Diffraction (XRD) to identify the phase formation in these layers. The  $2\theta$  range from 5° to 120° and Cu-K $\alpha$ 1 radiation are used on an X-ray diffraction instrument. The software GSAS-II [36] was used for the indexation of the XRD patterns obtained in this characterization.

### 3. Results and discussion

At first, the joint surfaces and cross-sections are investigated for varied process conditions, i.e. welding speed and tool rotational speed. All joints present a good surface finish, without lack-of-fill defect and flash, as shown by the representative macrograph in Fig. 2(a) of Weld 3. The joints present some dispersed steel fragments in the Al-SZ, which were detached by the probe contact to the steel surface and dragged upwards by the softened aluminum in movement around the tool. In this way, fewer steel particles are detached when the welding speed is increased or the rotational speed is decreased. Furthermore, two types of macrostructure features are observed in the weld cross-sections, which are the presence of a steel hook within the Al-SZ, Fig. 2(b)–(g), and tunnel defects, Fig. 2(d) and (f). The tunnel defect can be eliminated, and the steel hook can be significantly reduced by reducing welding and rotational speed, as shown in Fig. 2(g). The steel hook is also reduced in the welds that present tunnel defect. The different features are shown in detail in Fig. 3.

The formation of the steel hook within the Al-SZ, Fig. 3(a) and (b), is more evident on the RS and probably occurred due to the contact between the probe and the steel surface. Since the mixing of materials is less intense at high welding speeds, the steel hook is more evident in the joints produced using lower welding speeds in combination with a high rotational speed, i.e. welds 3, 4, 6 and 7, see Fig. 3(d). According to Xiong



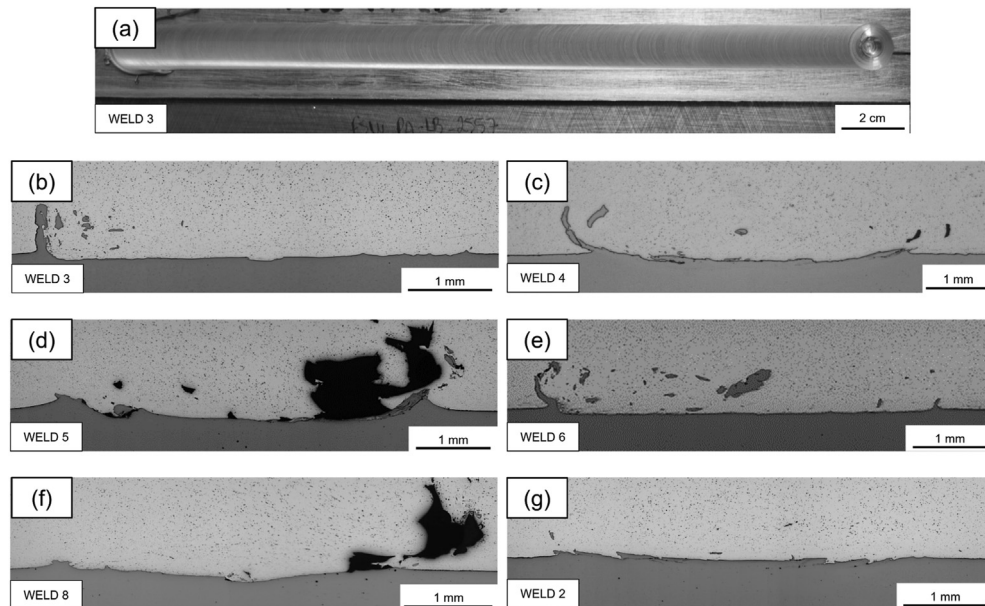


**Fig. 2 – (a) Visual inspection of the joint surface of Weld 3, using 700 rpm and 5 mm/s. Cross-section of the AA5083/GL D36 steel joints produced by FSW using different welding parameters: (b) Weld 3, i.e. 700 rpm and 5 mm/s, (c) Weld 4, i.e. 700 rpm and 9 mm/s, (d) Weld 5, i.e. 700 rpm and 13 mm/s, (e) Weld 6, i.e. 900 rpm and 5 mm/s, (f) Weld 8, i.e. 900 rpm and 13 mm/s, and (g) Weld 2, i.e. 500 rpm and 5 mm/s.**

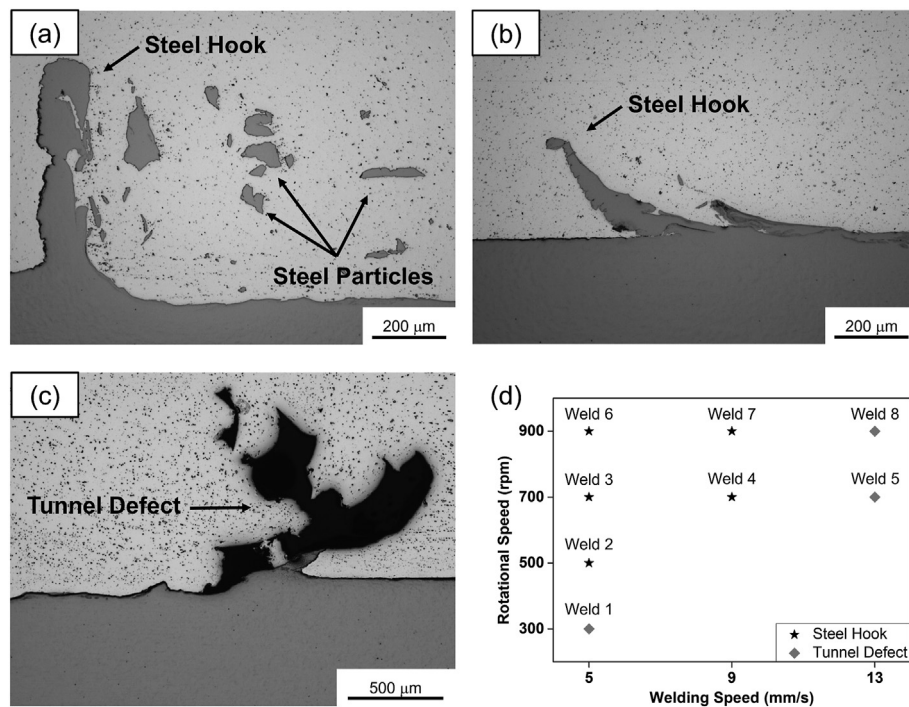


**Fig. 3 – Detailed view of formed steel hook in the joints of (a) Weld 3, i.e. 700 rpm and 5 mm/s, and (b) Weld 7, i.e. 900 rpm and 9 mm/s. (c) Tunnel defect in the cross-section of the joint of Weld 1, i.e. 300 rpm and 5 mm/s. (d) Occurring features, according to used welding parameters.**

et al. [31], as a consequence of the inversely proportional relationship between welding speed and energy input, the height of the steel hook decreases with increasing welding speed.

For high welding speeds, the height of the steel hook is significantly decreased, reducing from around 600 μm and 450 μm in the welds 3 and 6 (with 5 mm/s) respectively, to a minimum of 100 μm in the Weld 8 (with 13 mm/s), such as

reported by Xiong et al. [31]. This decrease of the steel hook height at high welding speed may be a result of the shorter dwell time at lower temperatures, which reduces the plastic deformation of the steel at the interface. Nonetheless, the height of the steel hook can vary throughout the length of the weld, since changes in temperature, time at a certain temperature, cooling rate, and thickness of the plastic zone transported by the probe can occur during the process, which also results in small deviations of the plunge depth. On the AS of welds 1, 5, and 8, tunnel defects were formed due to the insufficient energy input related to the low rotational speed, Fig. 3(c), or high welding speed, Fig. 2(d) and (f).

The microstructural features observed in the joints are shown in Fig. 4. The present different zones include the BMs, heat-affected zone (HAZ), and thermo-mechanically affected zone (TMAZ) in both aluminum and steel sides, and the SZ on the aluminum side, see Fig. 4(a).

AA5083-O/H111 is a non-heat treatable alloy, which has been annealed and strain hardened by rolling, resulting in a microstructure of the Al-BM with grains slightly elongated perpendicularly to the weld direction, and an average grain size of 35  $\mu\text{m}$ . Next to the Al-BM, the Al-HAZ is present,

which is affected only by the thermal cycle, which features a microstructure similar to the BM. The Al-TMAZ, which experienced both thermal cycle and plastic deformation, presents deformed and elongated grains. The Al-SZ is characterized by fine and equiaxed grains, dynamically recrystallized as a result of the FSW process. This zone also contains steel particles detached from the steel plate surface and exhibits grain sizes varying from around 4  $\mu\text{m}$ –12.7  $\mu\text{m}$ , depending on the process parameters. The grain size in the Al-SZ decreases slightly with decreasing rotational speed as well as with increasing welding speed, as summarized in Fig. 5.

The GL D36 steel is a high-strength steel with low carbon and high manganese contents, and niobium micro-alloying. The St-BM is supplied in rolled condition and characterized by a ferritic-perlitic microstructure. Since the probe just scratched the surface, but was not inserted into the steel plate during the FSW process, and since its melting point is significantly higher than the one of aluminum, there are no metallurgical changes detected during welding in the steel part, such as the formation of bainite and martensite. In this regard, a deformed microstructure is present in the St-TMAZ,

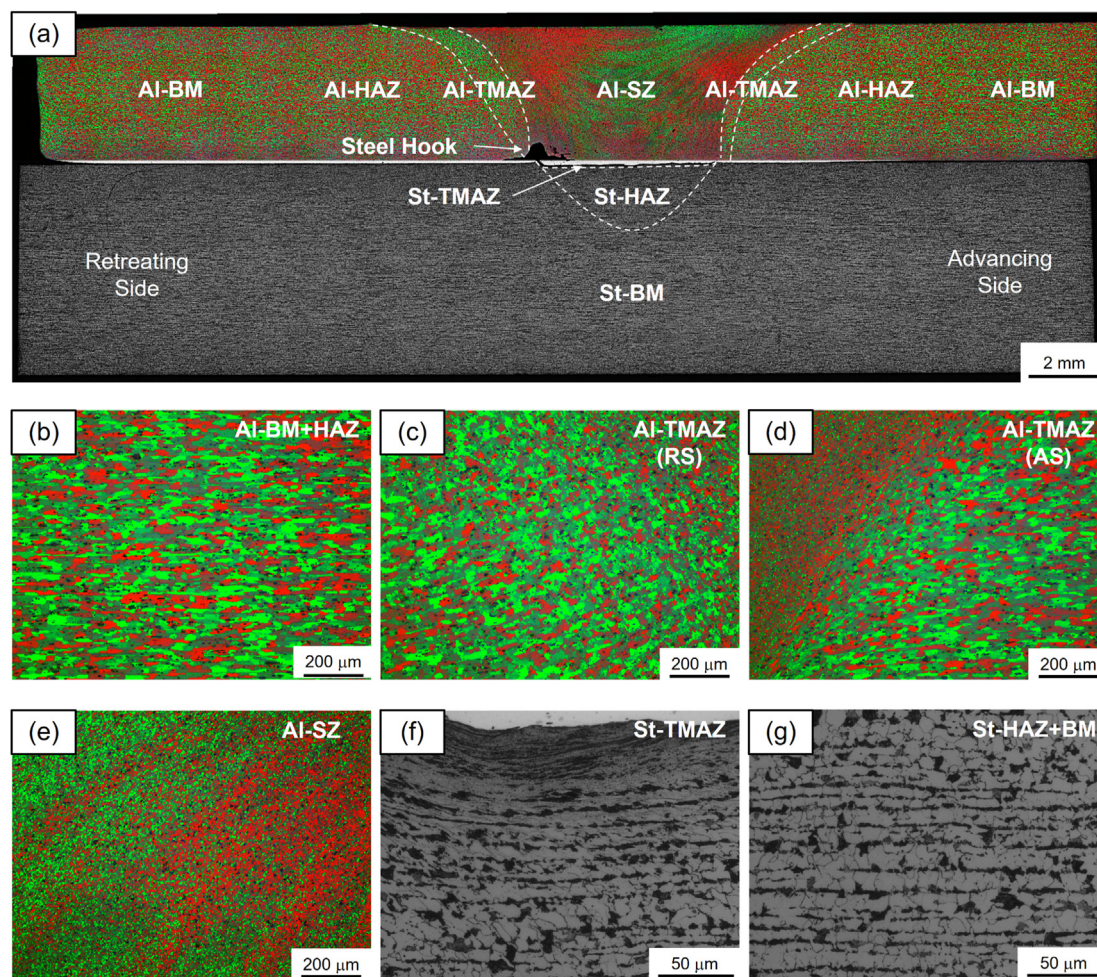


**Fig. 4 – (a) Microstructure of Weld 3 (rotational speed of 700 rpm and welding speed of 5 mm/s), and different weld zones: (b) aluminum BM and HAZ, (c) aluminum TMAZ on the retreating side, (d) aluminum TMAZ on the advancing side, (e) aluminum SZ, (f) steel TMAZ, and (g) steel BM and HAZ.**



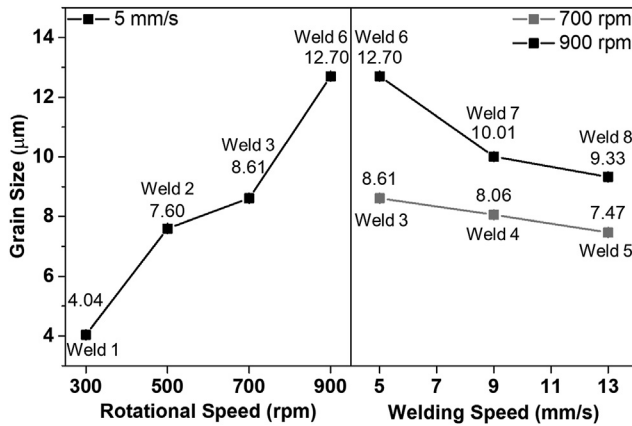


Fig. 5 – Average grain size in the Al-SZ for the different welds, representing different process parameters.

with elongated perlite and ferrite grains, while the St-HAZ exhibits still a microstructure similar to the St-BM.

The detailed SEM analyses reveal the presence of continuous IMC layers throughout the entire interface of the welds 3 (700 rpm and 5 mm/s), 4 (700 rpm and 9 mm/s), and 7 (900 rpm and 9 mm/s), as shown in Fig. 6, with an average thickness of around 250 nm, 400 nm, and 800 nm, respectively. As discussed by Wan et al. [34], the formation and growth of IMC layers are affected by the energy input and plastic deformation at the weld interface. The energy input in FSW is conventionally described by [37].

$$E_s = \frac{Q_{(total)}}{W_s} = \frac{M\omega}{W_s}, \quad (1)$$

whereby  $E_s$  represents the energy/heat input in [J/mm],  $M$  is the torque in [Nm],  $\omega$  is the rotational speed [rad] and  $W_s$  denotes welding speed [mm/s]. Another important factor

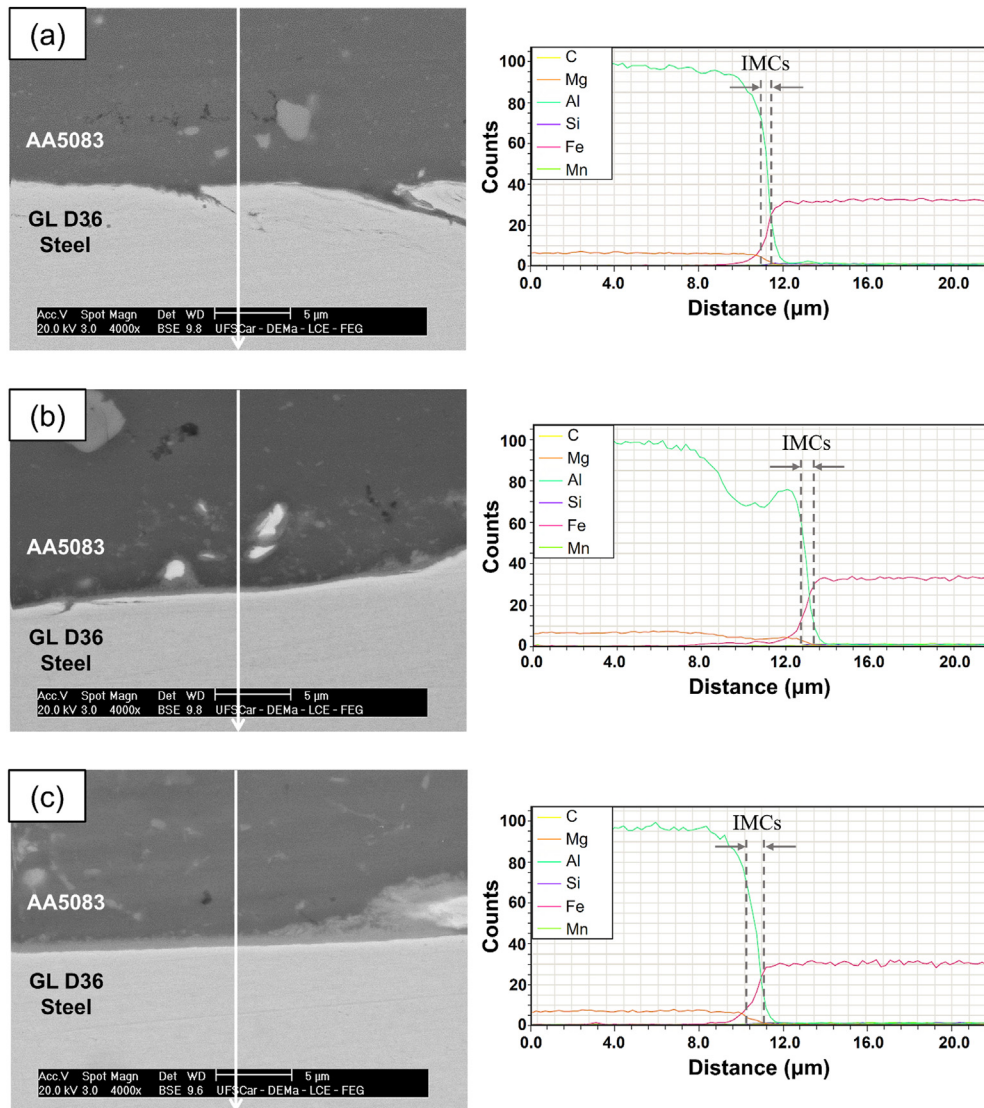


Fig. 6 – SEM backscattered micrographs and EDS line scan results of the joints interface of (a) Weld 3 (700 rpm and 5 mm/s), (b) Weld 4 (700 rpm and 9 mm/s), and (c) Weld 7 (900 rpm and 9 mm/s).

controlling material flow and temperature at the interface between materials in an overlap joint is the contact condition  $\delta$ , given by

$$\delta = \frac{\omega_{\text{shear layer}}}{\omega} \quad (2)$$

whereby  $\omega_{\text{shear layer}}$  is the rotational speed of the shear layer [rad].  $\delta = 0$  represents the case of “sliding”, where  $\delta = 1$  indicates “sticking”.

Depending on the contact condition between the tool and the BM (slipping or sticking), an increase in energy input results in an increase in the temperature in the SZ accompanied by an increase of the time at high temperatures and a slower cooling rate. This combined effects support the growth of IMC phases. In other words, the thicker IMC layer observed with the increase in rotational speed is a result of higher SZ temperatures coupled with a longer dwell time at higher

temperatures, which allows for diffusional growth. Similarly, increasing the welding speed leads to a reduction of the energy input. As a result the maximum temperatures reached at the SZ are lower, the time at temperature is reduced and the cooling rates faster. Consequently, thicker IMC layers are formed, and fewer steel particles detached from the interface, as can be seen in the cross-section of Weld 4, Fig. 2(c), when compared to Weld 3, Fig. 2(b), and as reported in the literature [30]. The detachment of more steel particles with decreasing the welding speed contributes to thinner IMC layers, in view that these layers are continuously broken and dispersed with steel particles.

Additionally, the difference in the mechanical properties between aluminum and steel produced micro interlocks in regions of the weld interface, as shown in Fig. 6(a). The lower ductility of the steel compared to aluminum resulted in irregularities and an increase in the surface roughness of the

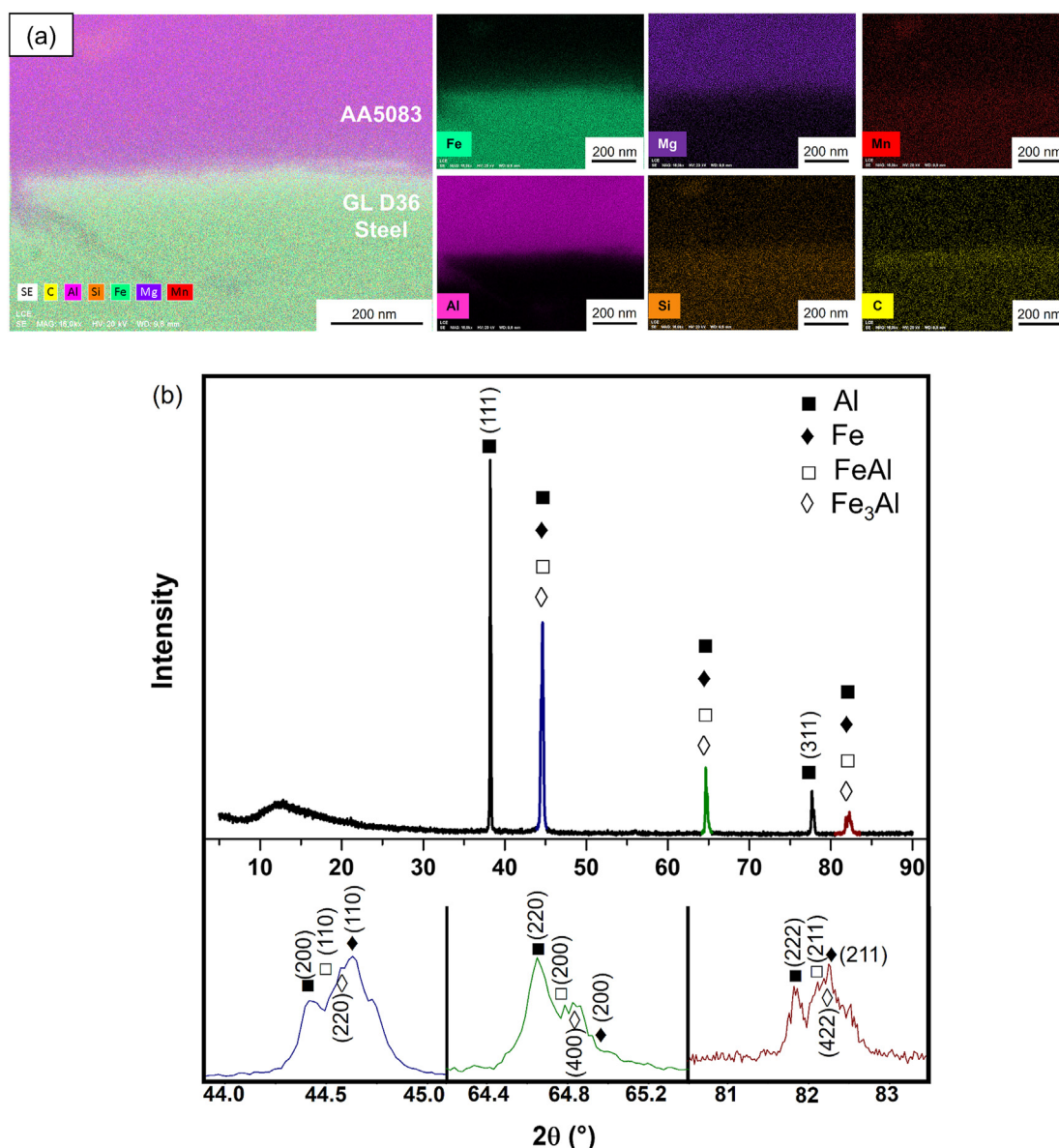


Fig. 7 – (a) EDS chemical maps of the IMC layer showing Fe, Mg, Mn, Al, Si, and C elements, and (b) X-ray diffraction pattern from the cross-section of Weld 3 (700 rpm and 5 mm/s).



steel at the interface, which was filled by the softened aluminum, forming micro interlocks with the reaction between aluminum and steel in the weld interface.

The chemical composition and phase formation of the IMC layer formed in Weld 3 is presented in Fig. 7. The EDS chemical composition maps, Fig. 7(a), show a mixture of Al and Fe atoms in the IMC layer, confirming the interdiffusion of them across the weld interface. In order to determine the phase formation in this IMC layer and around the steel particles in the Al-SZ, XRD patterns from the weld cross-section are analyzed, see Fig. 7(b). The diffraction lines can be attributed to the IMCs FeAl and Fe<sub>3</sub>Al, besides the Al and Fe structures from the base materials. These Fe-rich IMC phases are formed at the interface and around the steel particles dispersed in the Al-SZ. As mentioned earlier, these are less brittle than Al-rich phases and present good corrosion resistance properties. The FeAl phase is reported to form typically at around 1310 °C through a peritectic reaction, and Fe<sub>3</sub>Al through the first-order reaction of the FeAl phase at 552 °C under atmospheric pressure [38]. These phases have already been reported in the literature for dissimilar aluminum to steel FSW joints [30,38], and their formation at the present lower temperatures occur due to the present severe plastic deformation, which enhances the diffusion and the IMC nucleation and growth.

The microhardness measurements performed horizontally, i.e. in AA5083 and GL D36 steel side at a distance of 1 mm of the joint interface, as well as perpendicular to the weld interface are shown in Fig. 8. The AA5083 BM presents hardness values of around 86 HV<sub>0.2</sub>, which is determined by the grain size and content of solid solution elements. Since AA5083 belongs to the non-heat treatable aluminum alloys, the increased microhardness value measured in the Al-SZ is attributed to the grain refinement, Fig. 8(a). Therefore, higher microhardness values are reached at increasing welding and

decreasing rotational speeds, since this causes more pronounced strain rates and total strains, leading to smaller grain size dynamically recrystallized. The microhardness within the Al-SZ is almost constant, Fig. 8(a), with its maximum value of approximately 100 HV<sub>0.2</sub> for the Weld 1, i.e. 300 rpm and 5 mm/s. Due to the present deformation and resulting grain refinement in the TMAZ, the hardness in the Al-TMAZ is higher than in the Al-BM but smaller than in the Al-SZ. The Al-HAZ presents no significant differences to the hardness in the Al-BM due to the similarities in the microstructure of these regions [39,40].

The GL D36 steel BM presents hardness values of around 165 HV<sub>0.2</sub> that can be enhanced by strain hardening, refinement of ferrite and perlite grains, or by the formation of bainite and martensite [41]. No significant changes in microstructure are observed in the steel after the FSW process. The increases in microhardness in the St-TMAZ and St-HAZ occur due to the grain deformation and refinement as a result of the strain hardening, achieving a maximum hardness value of 208 HV<sub>0.2</sub> in the St-TMAZ of Weld 8, i.e. at 900 rpm and 13 mm/s, Fig. 8(a). The microhardness increases in particular near the interface, Fig. 8(b), due to the strain hardening of the steel and formation of IMCs, reaching hardness values of 356 HV<sub>0.2</sub> in the Weld 2, i.e. at 500 rpm and 5 mm/s.

The maximum lap shear loads determined for the different welds, respective samples, are presented in Fig. 9. All the samples were 25 mm wide and fractured in the weld interface due to the presence of brittle IMCs with high hardness. The maximum shear load of 16.98 kN is obtained for Weld 3, i.e. at a welding speed of 5 mm/s and a rotational speed of 700 rpm. Besides that, the shear load shows a tendency to increase with decreasing welding speed and increasing rotational speed up to 700 rpm, where the load is decreasing afterwards.

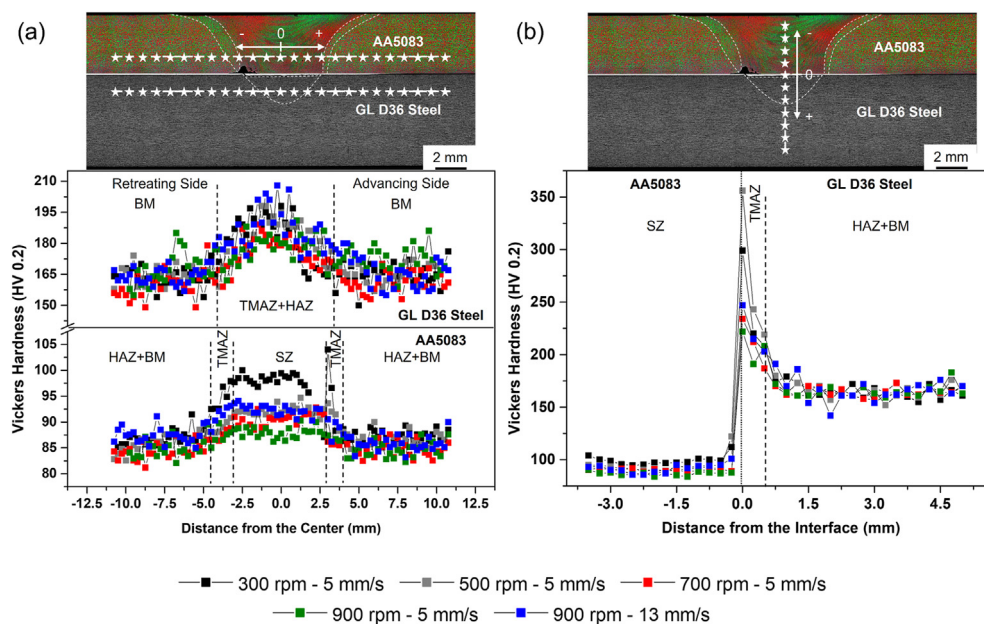


**Fig. 8 – (a) Vickers microhardness measurements, performed horizontal along the FSW cross-section of AA5083 and GL D36 steel at a distance of 1 mm to the interface, and (b) perpendicular to the weld cross-section in the center of the SZ of the joints. The welds were produced using different welding and rotational speeds.**

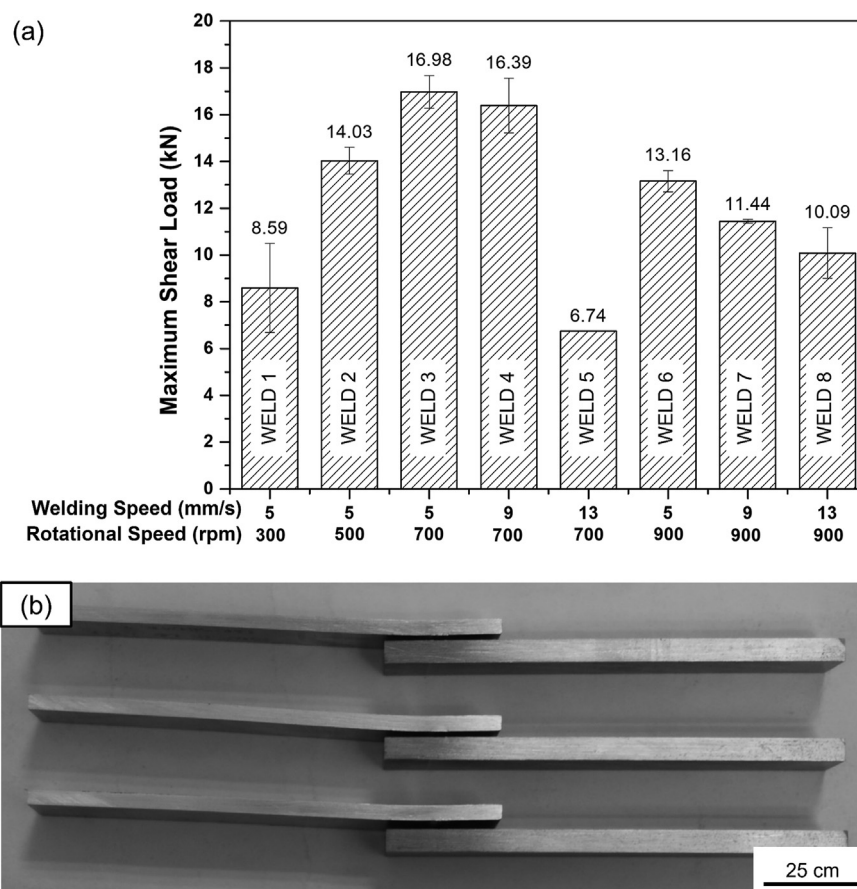


**Fig. 9 – (a) Effect of the rotational speed and welding speed on the lap shear strength of dissimilar AA5083/GL D36 lap welds, and (b) samples after the lap shear tests of the Weld 3, using a rotational speed of 700 rpm and welding speed of 5 mm/s.**

Among the results of the lap shear test, the welds 1, 5, and 8 present tunnel defects at the interface between aluminum and steel that reduce the width of the welded interface, resulting in the weakest performance in the lap shear tests, consistent with observations in the literature [30]. The degradation of the joint strength caused by tunnel defects can be confirmed with the higher lap shear load of Weld 2, which presents an almost flat interface, with a small steel hook, but without defects. The highest lap shear loads are obtained for welds 3 and 4, which exhibit steel hooks in the weld cross-section acting as macro interlocks. Numerical analysis of stress distribution during the lap shear tensile tests of adhesive lap joints already demonstrated that the maximum stress on the top plate occurs near the interface on the side of the joint where the load is being applied [42]. For example, when the aluminum plate is placed on the RS, the maximum stress in the aluminum takes place near the interface on the RS, i.e., near the steel hook, which consequently reduces the effective thickness of the top plate and the joint strength, as reported by Sorger et al. [33]. On the contrary, when the aluminum plate is placed on the AS, as used in the present study, the steel hook on the RS acts as mechanical interlocking, which is not detrimental to the joint strength.

However, differences in the maximum lap shear load are observed in the welds that show a steel hook. The welds 3 (Fig. 3a), 4 (Fig. 2c), and 7 (Fig. 3b) feature a macrostructure

characterized by the steel hook, but the lap shear load in these welds decreases with the increase of the rotational speed and welding speed, which is related to the increase of the IMC thickness. Besides that, Weld 3 presents micro interlocks in the interface, enhancing lap shear performance.

Therefore, macro and micro interlocks, and the formation of thin FeAl and Fe<sub>3</sub>Al intermetallic phases at the weld interface ensure sound mechanical and metallurgical bonding between aluminum and steel, resulting in higher mechanical properties of the welds, which is consistent with the results of the study of Movahedi et al. [32].

#### 4. Conclusions

Dissimilar AA5083-O/H111 and GL D36 steel welds were produced by FSW in a lap joint configuration with the aluminum plate placed on the AS, varying welding and tool rotational speeds. The main results of the microstructural and mechanical characterizations are summarized as follows:

- All welds possess good surface finishing and show plastically deformed steel particles dispersed in the Al-SZ. Two different features, the steel hook and tunnel defect, are observed in the macrostructure of the welds. The steel hook is more evident on the retreating side of the welds

produced using lower welding speeds, while the tunnel defect is present on the advancing side of the welds produced using high welding speed, i.e. 13 mm/s, or low rotational speed, i.e. 300 rpm.

- The Al-SZ consists of fine and equiaxed dynamic recrystallized grains. An increase in welding speed causes grain size reduction, where an increase in rotational speed leads to larger grain sizes, i.e. the resulting grain sizes are between 4 and 12.7  $\mu\text{m}$  in the aluminum stir zone.
- The interface of the welds are characterized by IMC layers composed of the Fe-rich phases FeAl and Fe<sub>3</sub>Al. The increase in the welding and rotational speed causes an increase in the average thickness of these layers from around 250 nm–800 nm, which contributes to the degradation of the lap shear strength, due to the brittleness and high hardness of these phases. Additionally, the different mechanical properties between aluminum and steel result in micro interlocks in the weld interface.
- The present macroscopic, microstructure, and interface features determine the resulting mechanical properties of the joints. The tunnel defects result in the deterioration of the lap shear strength of the welds, where the steel hook leads to higher lap shear strength. Additionally, the presence of micro interlocks and a thin IMC layer in the interface of the Weld 3 (700 rpm and 5 mm/s) leads to the highest obtained lap shear load of 16.98 kN. Therefore, the optimal mechanical properties are resulting from a combination of macro and micro interlocks and the formation of thin IMC layers.

## Declaration of Competing Interest

The authors declare that they have no known competing financial interests or personal relationships that could have appeared to influence the work reported in this paper.

## Acknowledgments

This study was financed in part by the Coordenação de Aperfeiçoamento de Pessoal de Nível Superior – Brasil (CAPES) – Finance Code 001. The authors also thank the grant #2019/04613–3, São Paulo Research Foundation (FAPESP).

## REFERENCES

- [1] Martinsen K, Hu SJ, Carlson BE. Joining of dissimilar materials. *CIRP Ann - Manuf Technol* 2015;64:679–99. <https://doi.org/10.1016/j.cirp.2015.05.006>.
- [2] Miller WS, Zhuang L, Bottema J, Wittebrood AJ, De Smet P, Haszler A, et al. Recent development in aluminum alloys for the automotive industry. *Mater Sci Eng, A* 2000;280(1):37–49. [https://doi.org/10.1016/S0921-5093\(99\)00653-X](https://doi.org/10.1016/S0921-5093(99)00653-X).
- [3] Gullino A, Matteis P, D'Aiuto F. Review of aluminum-to-steel welding technologies for car-body applications. *Metals* 2019;9(3):315. <https://doi.org/10.3390/met9030315>.
- [4] Chen T. Process parameters study on FSW joint of dissimilar metals for aluminum-steel. *J Mater Sci* 2009;44:2573–80. <https://doi.org/10.1007/s10853-009-3336-8>.
- [5] Kusuda Y. Honda develops robotized FSW technology to weld steel and aluminum and applied it to a mass-production vehicle. *Ind Robot* 2013;40:208–12. <https://doi.org/10.1108/01439911311309889>.
- [6] Ohhama S, Hata T, Yahaba T, Kobayashi T, Miyahara T, Sayama M. Application of an FSW continuous welding technology for steel and aluminum to an automotive subframe. *SAE* 2013. <https://doi.org/10.4271/2013-01-0372>. Technical Paper 2013-01-0372, 2013.
- [7] Mishra RS, Ma ZY. Friction stir welding and processing. *Mater Sci Eng R* 2005;50:1–78. <https://doi.org/10.1016/j.mser.2005.07.001>.
- [8] Prater T. Solid-state joining of metal matrix composites: a survey of challenges and potential solutions. *Mater Manuf Process* 2011;26:636–48. <https://doi.org/10.1080/10426914.2010.492055>.
- [9] Kashaev N, Ventzke V, Çam G. Prospects of laser beam welding and friction stir welding processes for aluminum airframe structural applications. *J Manuf Process* 2018;36:571–600. <https://doi.org/10.1016/j.jmapro.2018.10.005>.
- [10] Çam G, İpekoğlu G. Recent developments in joining of aluminum alloys. *Int J Adv Manuf Technol* 2017;91:1851–66. <https://doi.org/10.1007/s00170-016-9861-0>.
- [11] Çam G. Friction stir welded structural materials: beyond Al-alloys. *Int Mater Rev* 2011;56:1–48. <https://doi.org/10.1179/095066010X12777205875750>.
- [12] İpekoğlu G, Gören Kiral B, Erim S, Çam G. Investigation of the effect of temper condition on friction stir weldability of AA7075 Al-alloy plates. *Mater Technol* 2012;46:627–32.
- [13] İpekoğlu G, Erim S, Çam G. Investigation into the influence of post-weld heat treatment on the friction stir welded AA6061 Al-alloy plates with different temper conditions. *Metall Mater Trans* 2014;45:864–77. <https://doi.org/10.1007/s11661-013-2026-y>.
- [14] İpekoğlu G, Erim S, Gören Kiral B, Çam G. Investigation into the effect of temper condition on friction stir weldability of AA6061 Al-alloy plates. *Kovove Mater* 2013;51:155–63.
- [15] Von Strombeck A, Çam G, Dos Santos JF, Ventzke V, Koçak M. A comparison between microstructure, properties, and toughness behavior of power beam and friction stir welds in Al-alloys. In: Das SK, Kaufman JG, Lienert TJ, editors. *Proc of the TMS 2001 annual meeting aluminum, automotive and joining*; 2001 Feb 12–14; New Orleans, Louisiana, USA. Warrendale, PA, USA: TMS; 2001. p. 249–64.
- [16] İpekoğlu G, Erim S, Çam G. Effects of temper condition and post weld heat treatment on the microstructure and mechanical properties of friction stir butt-welded AA7075 Al alloy plates. *Int J Adv Manuf Technol* 2014;70:201–13. <https://doi.org/10.1007/s00170-013-5255-8>.
- [17] Çam G, İpekoğlu G, Serindağ HT. Effects of use of higher strength interlayer and external cooling on properties of friction stir welded AA6061-T6 joints. *Sci Technol Weld Join* 2014;19:715–20. <https://doi.org/10.1179/1362171814Y.0000000247>.
- [18] İpekoğlu G, Çam G. Effects of initial temper condition and postweld heat treatment on the properties of dissimilar friction-stir-welded joints between AA7075 and AA6061 aluminum alloys. *Metall Mater Trans* 2014;45:3074–87. <https://doi.org/10.1007/s11661-014-2248-7>.
- [19] Küçükömeroğlu T, Aktarer SM, İpekoğlu G, Çam G. Mechanical properties of friction stir welded St37 and St44 steel joints. *Mater Test* 2018;60:1163–70. <https://doi.org/10.3139/120.111266>.



- [20] İpekoğlu G, Küçükömeroğlu T, Aktarer SM, Sekban DM, Çam G. Investigation of microstructure and mechanical properties of friction stir welded dissimilar St37/St52 joints. *Mater Res Express* 2019;6:046537. <https://doi.org/10.1088/2053-1591/aafb9f>.
- [21] Bozkurt Y, Salman S, Çam G. Effect of welding parameters on lap-shear tensile properties of dissimilar friction stir spot welded AA5754-H22/2024-T3 joints. *Sci Technol Weld Join* 2013;18:337–45. <https://doi.org/10.1179/1362171813Y.0000000111>.
- [22] Kah P, Shrestha M, Martikainen J. Trends in joining dissimilar metals by welding. *Appl Mech Mater* 2013;440:269–76. <https://doi.org/10.4028/www.scientific.net/AMM.440.269>.
- [23] Mehta KP. A review on friction-based joining of dissimilar aluminum-steel joints. *J Mater Res* 2018;34:78–96. <https://doi.org/10.1557/jmr.2018.332>.
- [24] Schneider J, Radzilowski R. Welding of very dissimilar materials (Fe-Al). *J Occup Med* 2014;66:2123–9. <https://doi.org/10.1007/s11837-014-1134-5>.
- [25] Heidarzadeh A, Mironov S, Kaibyshev R, Çam G, Simar A, Gerlich A, et al. Friction stir welding/processing of metals and alloys: a comprehensive review on microstructural evolution. *Prog Mater Sci* 2020. <https://doi.org/10.1016/j.pmatsci.2020.100752>.
- [26] Taban E, Gould JE, Lippold JC. Dissimilar friction welding of 6061-T6 aluminum and AISI 1018 steel: properties and microstructural characterization. *Mater Des* 2010;31:2305–11. <https://doi.org/10.1016/j.matdes.2009.12.010>.
- [27] Kobayashi S, Yakou T. Control of intermetallic compound layers at interface between steel and aluminum by diffusion-treatment. *Mater Sci Eng, A* 2002;338:44–53. [https://doi.org/10.1016/S0921-5093\(02\)00053-9](https://doi.org/10.1016/S0921-5093(02)00053-9).
- [28] Kimapong K, Watanabe T. Lap joint of A5083 aluminum alloy and SS400 steel by friction stir welding. *Mater Trans* 2005;46:835–41. <https://doi.org/10.2320/matertrans.46.835>.
- [29] Coelho RS, Kostka A, Sheikh S, Dos Santos JF, Pyzalla AR. Microstructure and mechanical properties of an AA6181-T4 aluminum alloy to HC340LA high strength steel friction stir overlap weld. *Adv Eng Mater* 2008;10:961–72. <https://doi.org/10.1002/adem.200800028>.
- [30] Pourali M, Abdollah-zadeh A, Saeid T, Kargar F. Influence of welding parameters on intermetallic compounds formation in dissimilar steel/aluminum friction stir welds. *J Alloys Compd* 2017;715:1–8. <https://doi.org/10.1016/j.jallcom.2017.04.272>.
- [31] Xiong JT, Li JL, Qian JW, Zhang FS, Huang WD. High strength lap joint of aluminium and stainless steels fabricated by friction stir welding with cutting pin. *Sci Technol Weld Join* 2012;17:196–201. <https://doi.org/10.1179/1362171811Y.0000000093>.
- [32] Movahedi M, Kokabi AH, Seyed Reihani SM, Najafi H. Mechanical and microstructural characterization of Al-5083/St-12 lap joints made by friction stir welding. *Procedia Eng* 2011;10:3297–303. <https://doi.org/10.1016/j.proeng.2011.04.544>.
- [33] Sorger G, Wang H, Vilaça P, Santos TG. FSW of aluminum AA5754 to steel DX54 with innovative overlap joint. *Weld World* 2017;61:257–68. <https://doi.org/10.1007/s40194-016-0412-y>.
- [34] Wan L, Huang Y. Microstructure and mechanical properties of Al/steel friction stir lap weld. *Metals* 2017;7:542. <https://doi.org/10.3390/met7120542>.
- [35] Kimapong K, Watanabe T. Friction stir welding of aluminum alloy to steel. *Weld J* 2010;83:277S–82S.
- [36] Toby BH, Von Dreele RB. GSAS-II: the genesis of a modern open-source all purpose crystallography software package. *J Appl Crystallogr* 2013;46:544–9. <https://doi.org/10.1107/S0021889813003531>.
- [37] Schmidt HNB. Modeling thermal properties in friction stir welding. In: Lohwasser D, Chen Z, editors. *Friction stir welding: from basics to applications*. Woodhead Publishing Ltd.; 2010. p. 277–313.
- [38] Liu X, Lan S, Ni J. Analysis of process parameters effects on friction stir welding of dissimilar aluminum alloy to advanced high strength steel. *Mater Des* 2014;59:50–62. <https://doi.org/10.1016/j.matdes.2014.02.003>.
- [39] Gungor B, Kaluc E, Taban E, Sik A. Mechanical, fatigue and microstructural properties of friction stir welded 5083-H111 and 6082-T651 aluminum alloys. *Mater Des* 2014;56:84–90. <https://doi.org/10.1016/j.matdes.2013.10.090>.
- [40] Threadgill PL, Leonard AJ, Shercliff HR, Withers PJ. Friction stir welding of aluminium alloys. *Int Mater Rev* 2009;54:49–93. <https://doi.org/10.1179/174328009X411136>.
- [41] Reynolds AP, Tang W, Posada M, Deloach J. Friction stir welding of DH36 steel. *Sci Technol Weld Join* 2003;8:455–60. <https://doi.org/10.1179/136217103225009125>.
- [42] Guilpin A, Franciere G, Barton L, Blacklock M, Birkett M. A numerical and experimental study of adhesively-bonded polyethylene pipelines. *Polymers* 2019;11:1531. <https://doi.org/10.3390/polym11091531>.